

Supplementary Information

A multifunctional hole-transporter for high-performance TADF OLEDs and clarification of factors governing the transport property by multiscale simulation

*Natsuo Nagamura¹, Hisahiro Sasabe^{*1,2,3}, Hiroki Sato⁴, Takahiro Kamata¹, Nozomi Ito¹, Suguru Araki¹, Shoki Abe¹, Yoshihito Sukegawa¹, Daisuke Yokoyama^{1,2}, Hironori Kaji^{*4}, Junji Kido^{*1,2,3}*

¹Department of Organic Materials Science, Yamagata University, 4-3-16 Jonan, Yonezawa, Yamagata 992-8510, Japan, ²Research Center of Organic Electronics (ROEL), Yamagata University, 4-3-16 Jonan, Yonezawa, Yamagata 992-8510, Japan, ³Frontier Center for Organic Materials (FROM), Yamagata University, 4-3-16 Jonan, Yonezawa, Yamagata 992-8510, Japan,

⁴Institute for Chemical Research, Kyoto University Uji, Kyoto 611-0011, Japan

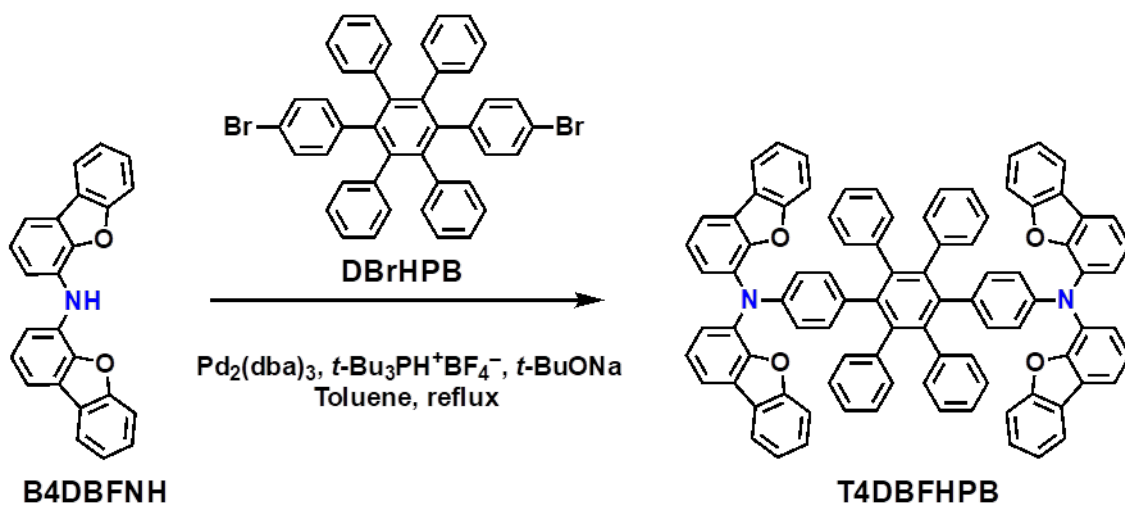
E-mail: h-sasabe@yz.yamagata-u.ac.jp; kaji@scl.kyoto-u.ac.jp; kid@yz.yamagata-u.ac.jp

General Considerations:

Quantum chemical calculations were performed using the hybrid density functional theory (DFT), functional Becke and Hartree-Fock exchange, and Lee Yang and Parr correlation (B3LYP) as implemented in the Gaussian 09 program packages.^[1] Electrons were described by the Pople 6-31G(d,p) and 6-311+G(d,p) basis sets for molecular structure optimization and single-point energy calculations, respectively. The BDEs of the anion states were calculated at the URB3LYP 6-31G(d) level of theory according to the enthalpy change in the corresponding reaction of homolytic cleavage of a single bond in the gas phase at 298 K and 1 atm.^[2] ¹H-NMR and ¹³C-NMR spectra were recorded on a JEOL 400 and a JEOL 600 spectrometer. Mass spectra were obtained using a JEOL JMS-K9 mass spectrometer and a Waters SQD2 mass spectrometer with atmospheric pressure solid analysis probe (ASAP). Differential scanning calorimetry (DSC) was performed using a Perkin-Elmer DSC 8000 Pyris instrument under nitrogen atmosphere at a heating rate of 10°C min⁻¹. Thermogravimetric analysis (TGA) was undertaken using a Perkin-Elmer TGA 4000 unit under nitrogen atmosphere at a heating rate of 10°C min⁻¹. UV-Vis spectra were measured using a Shimadzu UV-2600 UV-vis spectrophotometer. Photoluminescence spectra were measured using a FluroMax-2 (Jobin-Yvon-Spex) luminescence spectrometer. The ionization potential (*I_p*) was determined using a photoelectron yield spectroscopy (PYS) in vacuum (~10⁻³ Pa).^[3] The phosphorescent spectra were measured using a streak camera (C4334 from Hamamatsu Photonics) at 6K.

References

- [1] Gaussian 09, Revision D.01, M. J. Frisch, G. W. Trucks, H. B. Schlegel, G. E. Scuseria, M. A. Robb, J. R. Cheeseman, G. Scalmani, V. Barone, B. Mennucci, G. A. Petersson, H. Nakatsuji, M. Caricato, X. Li, H. P. Hratchian, A. F. Izmaylov, J. Bloino, G. Zheng, J. L. Sonnenberg, M. Hada, M. Ehara, K. Toyota, R. Fukuda, J. Hasegawa, M. Ishida, T. Nakajima, Y. Honda, O. Kitao, H. Nakai, T. Vreven, J. A. Montgomery, Jr., J. E. Peralta, F. Ogliaro, M. Bearpark, J. J. Heyd, E. Brothers, K. N. Kudin, V. N. Staroverov, R. Kobayashi, J. Normand, K. Raghavachari, A. Rendell, J. C. Burant, S. S. Iyengar, J. Tomasi, M. Cossi, N. Rega, J. M. Millam, M. Klene, J. E. Knox, J. B. Cross, V. Bakken, C. Adamo, J. Jaramillo, R. Gomperts, R. E. Stratmann, O. Yazyev, A. J. Austin, R. Cammi, C. Pomelli, J. W. Ochterski, R. L. Martin, K. Morokuma, V. G. Zakrzewski, G. A. Voth, P. Salvador, J. J. Dannenberg, S. Dapprich, A. D. Daniels, Ö. Farkas, J. B. Foresman, J. V. Ortiz, J. Cioslowski, and D. J. Fox, Gaussian, Inc., Wallingford CT, 2013.
- [2] (a) N. Lin, J. Qiao, L. Duan, L. Wang, Y. Qiu, *J. Phys. Chem. C* **2014**, *118*, 7569. (b) M. Hong, M. K. Ravva, R. Winget, J.-L. Bredas, *Chem. Mater.* **2016**, *28*, 5791.
- [3] H. Ishii, D. Tsunami, T. Suenaga, N. Sato, Y. Kimura, M. Niwano, *J. Surf. Sci. Soc. Jpn.* **2007**, *28*, 264.



Scheme S1. Synthetic route of **T4DBFHPB**

Synthesis of T4DBFHPB:

B4DBFNH (350 mg, 1.0 mmol), **DBrHPB** (346 mg, 0.5 mmol), sodium-*t*-butoxide (250 mg, 2.6 mmol) and dry toluene (10 mL) were added into a three-necked flask and then, nitrogen (N₂) was bubbled through the mixture for 1h. After that, Pd₂(dba)₃ (45.8 mg, 0.05 mmol) and tri-*t*-butylphosphonium tetra-fluoroborate (29 mg, 0.1 mmol) were added and the resultant mixture was stirred for 20 h at the reflux temperature under the N₂ flow. Elimination of the ingredients and the spot of the target compound (R_f = 0.18) were confirmed in Thin-Layer Chromatography (TLC) (toluene/hexane=1/1 v/v). After cool this to room temperature, extractions were done with toluene for three times and the organic layer was dried, filtered, and condensed by magnesium sulfate (anhydrous). The obtained brown viscous body was solved in toluene (100 mL) and was purified by chromatography on silica gel (toluene/hexane=1/1 v/v). Finally, **T4DBFHPB** (470 mg, 78%) was obtained as a white solid. The target compound was identified from the results from ¹H-NMR, ¹³C-NMR, MS, and elemental analysis.

¹H NMR (400 MHz, CDCl₃) δ = 7.90 (d, J = 7.8 Hz, 4H), 7.66 (dd, J = 7.5, 1.1 Hz, 4H), 7.39-7.35 (m, 4H), 7.31-7.27 (m, 8H), 7.15 (t, J = 7.8 Hz, 4H), 6.97-6.84 (m, 24H), 6.70-6.67 (m, 4H), 6.57 (dd, J = 6.6, 2.1 Hz, 4H); ¹³C NMR (100 MHz, CDCl₃) δ = 156.06, 149.95, 143.95, 140.93, 140.50, 140.28, 135.48, 132.08, 131.90, 131.71, 126.98, 126.78, 125.87, 125.24, 124.40, 123.36, 123.25, 122.71, 120.72, 120.60, 116.07, 112.25, 77.48, 77.16, 76.84 ppm; MS: *m/z* 1230 [M + H]⁺; Elemental analysis (%) calculated for C₉₀H₅₆N₂O₄: C 87.92, H 4.59, N 2.28; found: C 87.84, H 4.58, N 2.30.

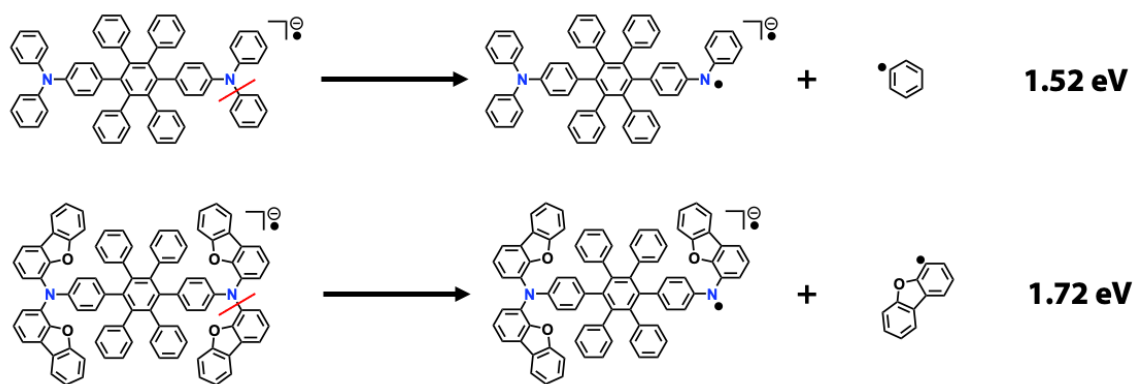


Figure S1. BDEs of TATT and T4DBFHPB.

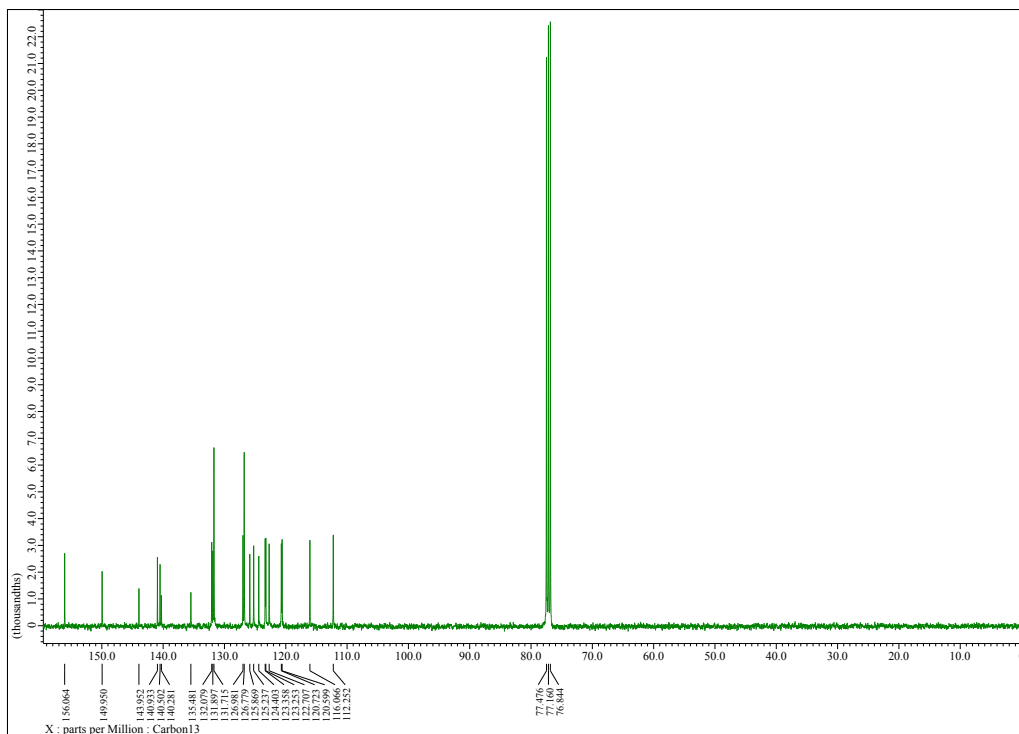


Figure S3. ^{13}C -NMR spectrum of **T4DBFHPB** (100 MHz, CDCl_3 , @R.T.)

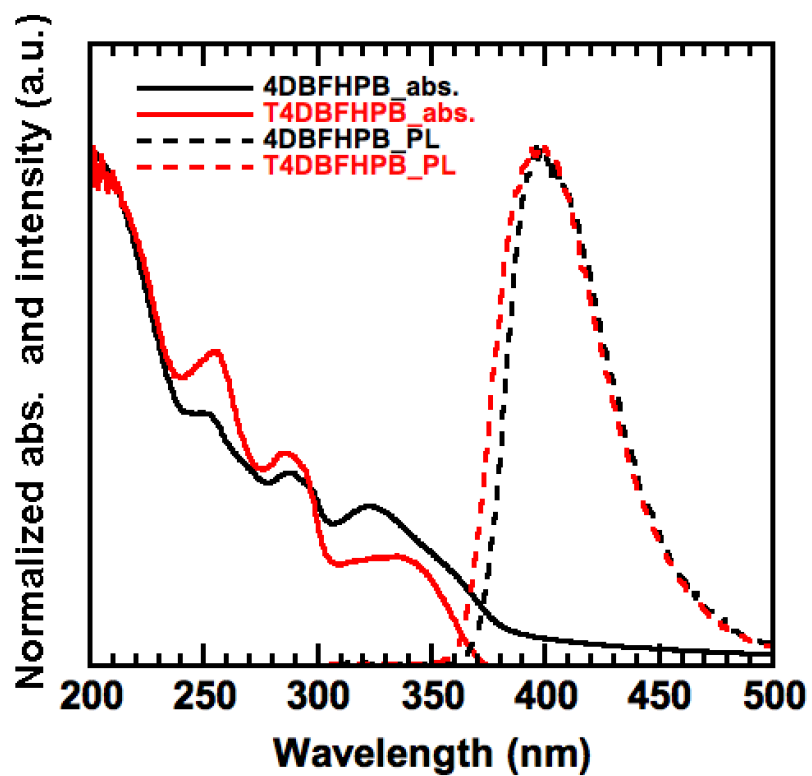


Figure S4. UV-vis absorption spectra and PL spectra of **4DBFHPB** and **T4DBFHPB** films.

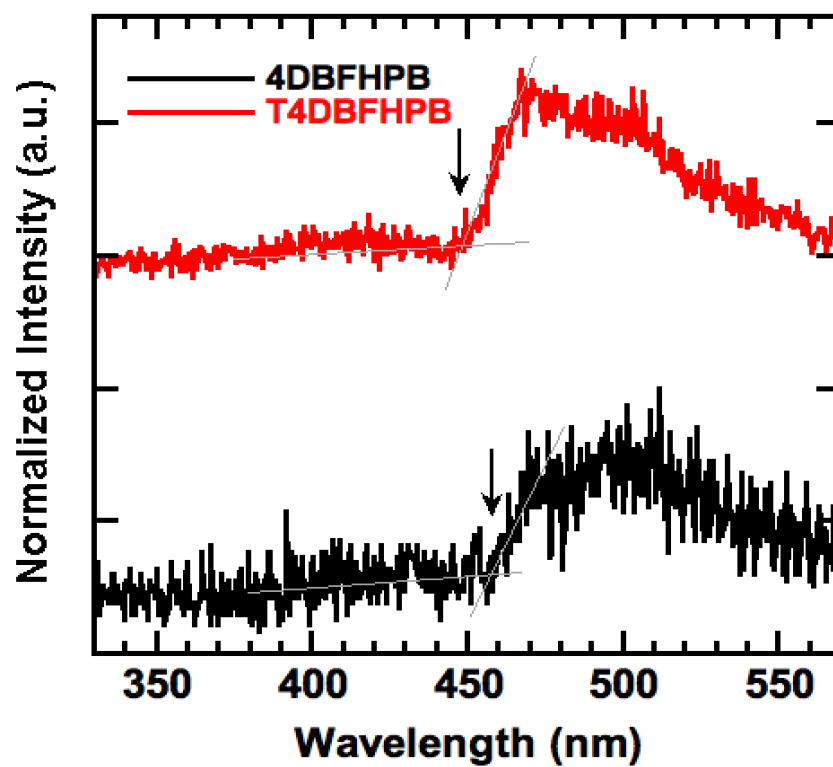


Figure S5. Phosphorescent spectra of 4DBFHPB and T4DBFHPB films.

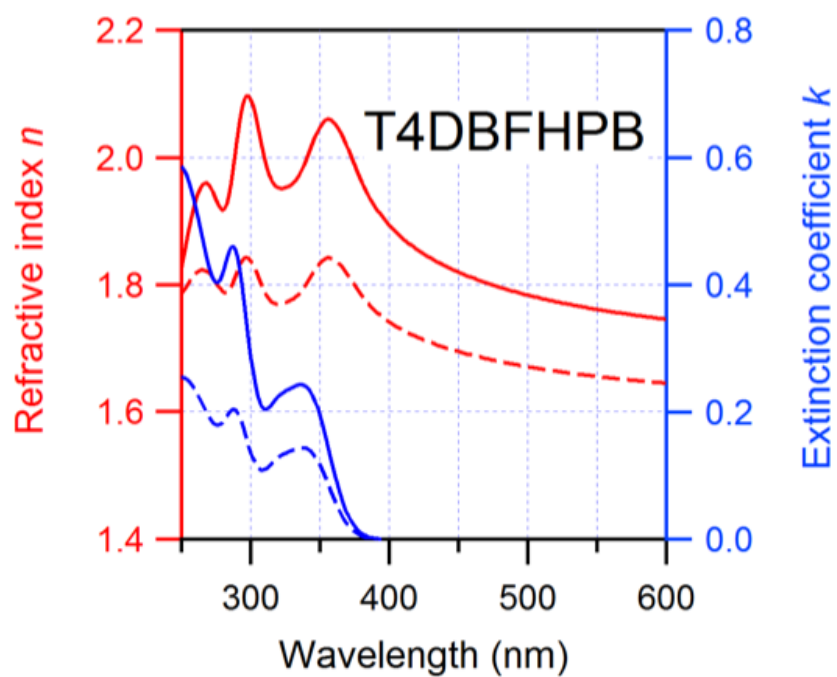


Figure S6. Anisotropies of the refractive indices and extinction coefficients of **T4DBFHPB**. The solid and broken lines indicate the horizontal and vertical components of the optical constants, respectively.

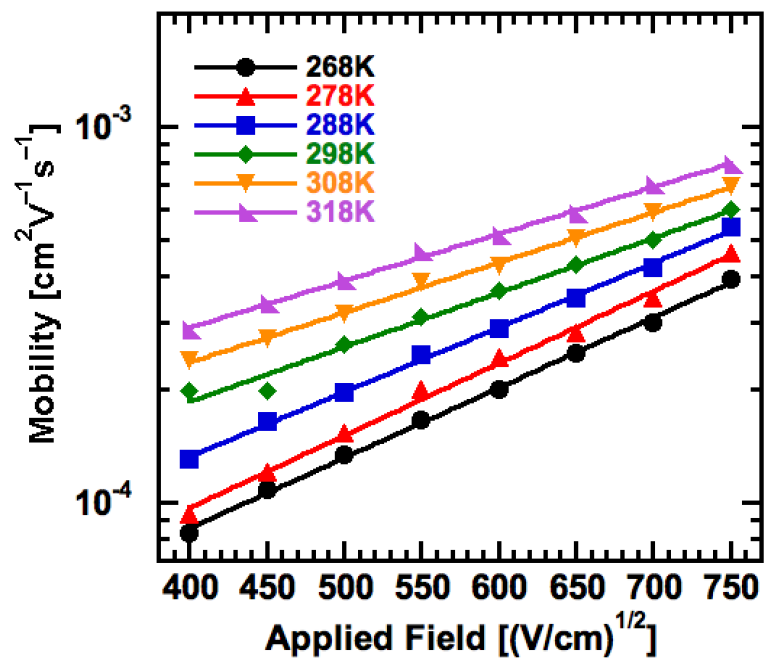


Figure S7. The temperature dependence of field-dependent hole-mobility of T4DBFHPB.

Theoretical detail for multiscale simulation

1. Density

The densities of the molecules estimated from MD calculation were 0.95, 1.11 (g cm⁻³) in **4DBFHPB** and **T4DBFHPB** respectively.

2. Site energy

Site energies of the i th molecule for HOMO $-p$ and LUMO $+p$ are defined as

$$E_i^{\text{H}-p} = \Delta\epsilon_i - \epsilon_i^{\text{H}-p}, \quad E_i^{\text{L}+p} = \Delta\epsilon_i + \epsilon_i^{\text{L}+p}.$$

Where, $\epsilon_i^{\text{H}-p}$ and $\epsilon_i^{\text{L}+p}$ are the eigenvalues of HOMO $-p$ and LUMO $+p$, respectively.

$\Delta\epsilon_i$ is the energy difference between charged state and neutral state:

$$\Delta\epsilon_i = \epsilon_{i,\text{Coulomb}}^{+(-)} - \epsilon_{i,\text{Coulomb}}^0$$

Electrostatic interaction with bare neighboring neutral molecules $\epsilon_{i,\text{Charge-charge}}$ and

the polarization effect $\epsilon_{i,\text{Charge-Dipole}}$ were taken into account:

$$\epsilon_{i,\text{Coulomb}}^{0/+/-} = \epsilon_{i,\text{Charge-charge}}^{0/+/-} + \epsilon_{i,\text{Charge-charge}}^{0/+/-}$$

Where,

$$\epsilon_{i,\text{Charge-charge}} = \sum_{j \neq i} \sum_{k_i} \sum_{k_j} \frac{1}{4\pi\epsilon_0} \frac{q_{i,k_i} q_{j,k_j}}{|\mathbf{r}_{ij,k_i,k_j}|}$$

$$\epsilon_{i,\text{Charge-Dipole}} = \sum_{j \neq i} \sum_{k_i} \sum_{k_j} -\frac{q_{i,k_i} \boldsymbol{\mu}_{j,k_j} \cdot \mathbf{r}_{ij,k_i,k_j}}{4\pi\epsilon_0 |\mathbf{r}_{ij,k_i,k_j}|^3}.$$

The summation of the index k_i runs over the all atoms of the i th molecule. We call

$\epsilon_i^{\text{H-P}}$ and $\Delta\epsilon_i$ *intramolecular site energy* and *intermolecular site energy* respectively.

In order to compare the contribution of permanent dipole moment and molecular polarization, we decomposed $\Delta\epsilon_i$ into $\Delta\epsilon_{i,\text{Charge-Charge}}$ and $\Delta\epsilon_{i,\text{Charge-Dipole}}$ in following manner:

$$\begin{aligned}\Delta\epsilon_i &= \epsilon_{i,\text{Coulomb}}^+ - \epsilon_{i,\text{Coulomb}}^0 \\ &= (\epsilon_{i,\text{Charge-Charge}}^+ - \epsilon_{i,\text{Charge-Charge}}^0) \\ &\quad + (\epsilon_{i,\text{Charge-Dipole}}^+ - \epsilon_{i,\text{Charge-Dipole}}^0) \\ &= \Delta\epsilon_{i,\text{Charge-Charge}} + \Delta\epsilon_{i,\text{Charge-Dipole}}.\end{aligned}$$

4. Governing factors for the difference between the hole-mobilities of **T4DBFHPB** and **4DBFHPB**.

In order to evaluate the contributions of the mobility factors quantitatively, we carried out kMC simulations with each factor varied. For molecules A and B, each factor indexed by $i = 1, 2, \dots, K$ takes two conditions. One is the unique condition from the molecules and the other is a standard condition. Namely, the variations of simulated mobilities of molecules A and B are

$$\mu_A(p_1^A, p_2^A, \dots, p_K^A), \mu_B(p_1^B, p_2^B, \dots, p_K^B) \quad (p_i^{A,B} = \text{Unique}_i^{A,B}, \text{Standard}_i^{A,B}). \quad (3.1)$$

In our analysis, the four factors ($K = 4$) are considered: Electronic coupling, intramolecular site energy, intermolecular site energy, and reorganization energy. Our purpose is to evaluate the contributions of these factors to following quantity:

$$\begin{aligned}y(p_1, p_2, \dots, p_K) &= \log_{10} \mu_B(p_1^B, p_2^B, \dots, p_K^B) - \log_{10} \mu_A(p_1^A, p_2^A, \dots, p_K^A) \\ &\quad (p_i = \text{Unique}_i, \text{Standard}_i) \quad (3.2)\end{aligned}$$

The “difference” between the mobilities of molecule A and B is measured from this quantity. $p_i = \text{Unique}_i, \text{Standard}_i$ means $(p_i^A, p_i^B) = (\text{Unique}_i^A, \text{Unique}_i^B), (\text{Standard}_i^A, \text{Standard}_i^B)$. Common standard conditions of molecules A and B are desirable and \mathbf{y} should be close to zero when the all factors are in the standard conditions. So, we set following standard conditions for our case of A = **4DBFHPB** and B = **T4DBFHPB**: As the standard condition of the electronic couplings, we took 1 meV for all of the connected pairs which any of H^{pq} is non zero. Actually, when we consider the fixed trajectories (this is the case of the random seeds of the kMC simulations are fixed) \mathbf{y} doesn’t depend on how to take the standard value of the electronic coupling. For the intramolecular and intermolecular site energy, we took the mean values of all of the sites for each orbital. Compared to these standard conditions of the three factors, standard conditions of the reorganization energy have some arbitrariness. We compared the cases in which all of the connected pairs take the same standard value $\lambda_{\text{standard}}$ of 100 meV and 155 meV (the intermediate value of the calculated reorganization energies of **4DBFHPB** and **T4DBFHPB**).

Then, we turn to the discussion of the contributions of the factors. **Figure S12** and **Figure S13** are the simulated hole-mobilities in the all-factors-are-standard and one-factor-is-unique conditions. From the top (**4DBFHPB**) and middle (**T4DBFHPB**) figures, we can see the effect of the changes of each factor from the standard condition to the unique condition. And from the bottom figure, we can check that the mobilities in the all-factors-are-standard condition are almost same value in **4DBFHPB** and **T4DBFHPB** for whole region of the applied field. When the mobilities of **4DBFHPB** and **T4DBFHPB** are considered separately, the effects of the each factor depend on how to take the standard conditions (Compare **Figure S12** and **Figure S13**). On the other hand, the effects to the difference \mathbf{y} should not depend on how to take the standard conditions. **Figure S14** shows the effects to the difference. In both figures a) and b), the effects of the electronic coupling and the intramolecular site energy are proved to be

advantageous in **T4DBFHPB** ($\mu_{\text{T4DBFHPB}}/\mu_{\text{4DBFHPB}} > 1$) and those of the others are proved to be disadvantageous ($\mu_{\text{T4DBFHPB}}/\mu_{\text{4DBFHPB}} < 1$). This evaluation satisfies the demand that the contributions should not depend on how to take the standard conditions. However, this is nothing but the result from “the conditions neighboring the all-factors-are-standard condition”. For example, we can also consider the case of “the conditions neighboring the all-factors-are-unique condition”. The results are shown in **Figure S15, S16** and **S17**. **Figure S17** indicates that all factors are disadvantageous ($\mu_{\text{T4DBFHPB}}/\mu_{\text{4DBFHPB}}$ is increased by changing each factor from the unique condition to the standard condition) in **T4DBFHPB** and this result is different from that of **Figure S17**. In spite of this difference, these two results indicate in common that the intermolecular site energy and the reorganization energy are the main factors that cause the inferior mobility in **T4DBFHPB**. These results are also consistent with the result of following analysis that was discussed in the main text:

In order to take into account all of the values of $y(p_1, p_2, \dots, p_K)$, we carried out the analysis of variance. [1] The contribution of the factor i to y is defined as follow:

$$v_i = \sum_{l_i} (\bar{x}_i(l_i) - \bar{x}_a)^2 / 2$$

Where, $\bar{x}_a = \sum_p y(p) / 2^K$ ($p = (p_1, p_2, \dots, p_K)$) is the grand mean and $\bar{x}_i(l_i) = \sum_{\{p|p_i=l_i\}} y(p) / 2^{K-1}$ is the mean of the condition p_i at l_i . If $\bar{x}_i(\text{Unique}_i) - \bar{x}_i(\text{Standard}_i)$ is positive (negative), the contribution of the factor i is positive (negative): In other word, molecule B is more advantageous (disadvantageous) than molecule A in terms of factor i for the mobility.

Finally, we made **Table 3** and **Figure S19** from the percentage contribution of each factor:

$$I_i = \frac{v_i}{\sum_{j=1}^K v_K} \times 100 \%$$

[1] B. Cao, L. A. Adutwum, A. O. Oliynyk, E. J. Lubber, B. C. Olsen, A. Mar and J. M. Buriak, ACS Nano 12 (8), **2018**, 7434

Table S1. Number of hops from HOMO- p to HOMO- q summed over all possible molecular pairs. All values are averaged over 30,000 trials of the kMC simulation at $F^{1/2} = 800 \text{ (V/cm)}^{1/2}$.

4DBFHPB

	HOMO	HOMO-1	HOMO-2	HOMO-3
HOMO	6823.3	4605.1	0.03	0.008
HOMO-1	4605.5	1963.1	0.08	0.02
HOMO-2	0.4	0.7	1.6	1.2
HOMO-3	0.2	0.4	1.4	1.2

T4DBFHPB

	HOMO	HOMO-1	HOMO-2	HOMO-3
HOMO	21033.3	7135.5	0.01	0.003
HOMO-1	7136.1	4605.3	0.04	0.005
HOMO-2	0.3	0.6	1.2	0.8
HOMO-3	0.2	0.4	1.0	1.3

Table S2. Mean values and standard deviations (std) of the site energies.

4DBFHPB

	Mean (eV)	Std (meV)
ϵ_i^{H-p} ($p = 0,1,2,3$)	11.5/11.6/12.0/12.0	22.8/32.4/28.6/22.6
$\Delta\epsilon_i$	-1.59	104
$\Delta\epsilon_{i,\text{Charge- Charge}}$	-0.135	68.5
$\Delta\epsilon_{i,\text{Charge- Dipole}}$	-1.45	90.7
E_i^{H-p} ($p = 0,1,2,3$)	9.92/9.96/10.4/10.4	106/109/111/108

T4DBFHPB

	Mean (eV)	Std (meV)
ϵ_i^{H-p} ($p = 0,1,2,3$)	11.4/11.5/11.9/12.0	13.5/11.5/30.6/21.8
$\Delta\epsilon_i$	-1.44	118
$\Delta\epsilon_{i,\text{Charge- Charge}}$	-0.186	82.5
$\Delta\epsilon_{i,\text{Charge- Dipole}}$	-1.26	91.0
E_i^{H-p} ($p = 0,1,2,3$)	10.0/10.0/10.5/10.6	119/118/124/121

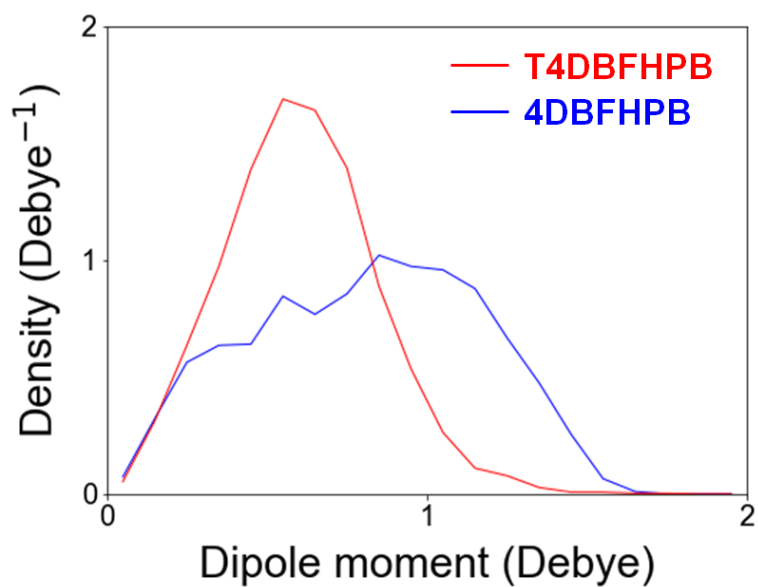


Figure S8. The distribution of the different values in dipole moments. The dipole moments were calculated from Merz-Singh-Kollman (MK) charges. The mean values were 0.81 Debye for **4DBFHPB** and 0.60 Debye for **T4DBFHPB**.

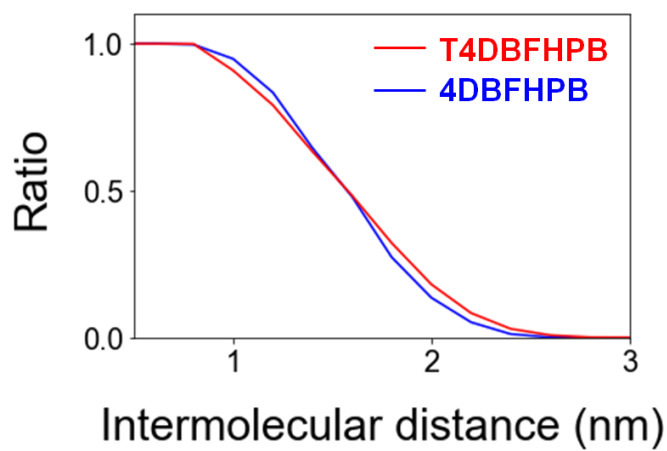


Figure S9. The ratio of the connected pairs to all of the pairs vs. intermolecular distance.

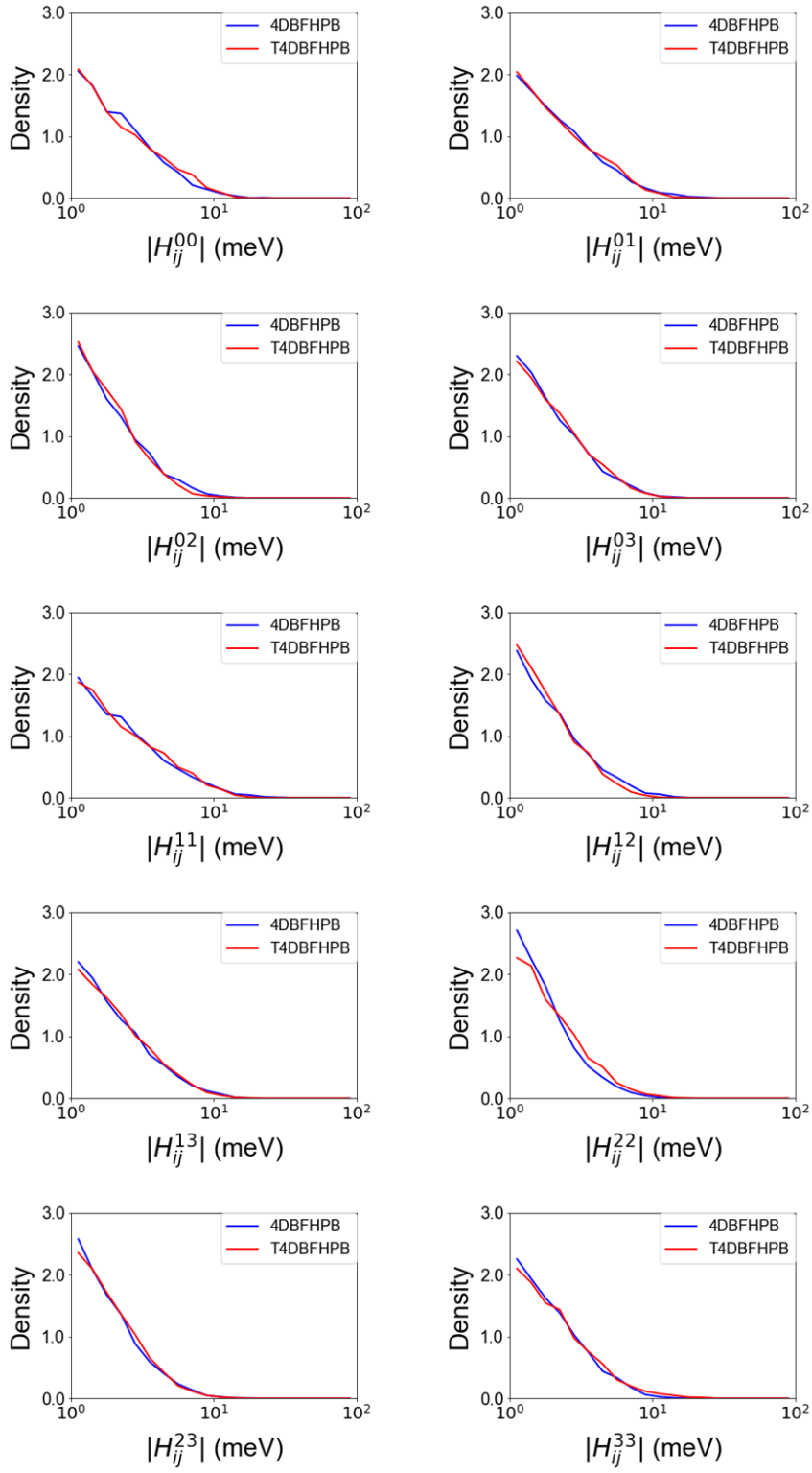


Figure S10. Distributions of H_{ij}^{pq} .

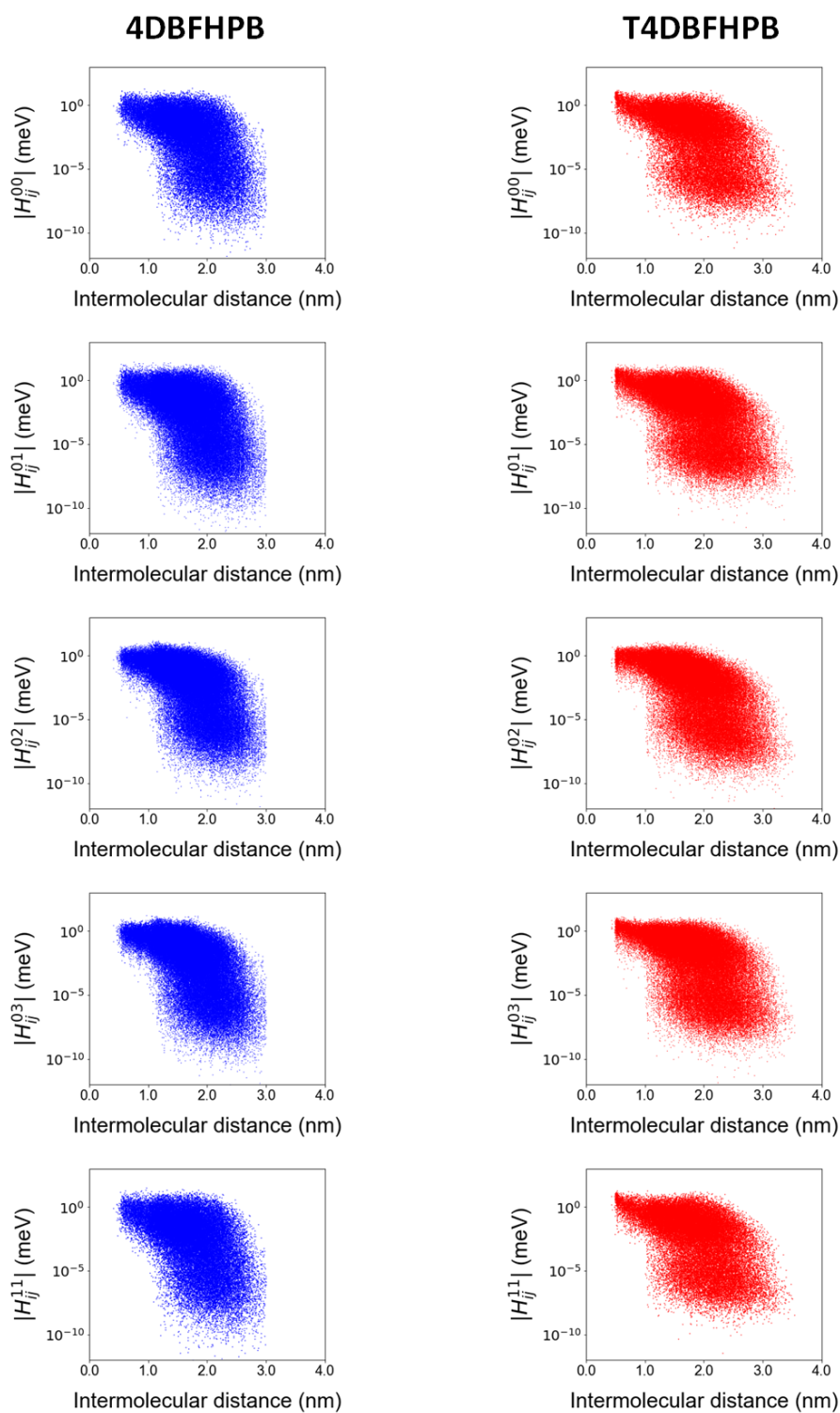


Figure S11. H_{ij}^{pq} vs. intermolecular distance.

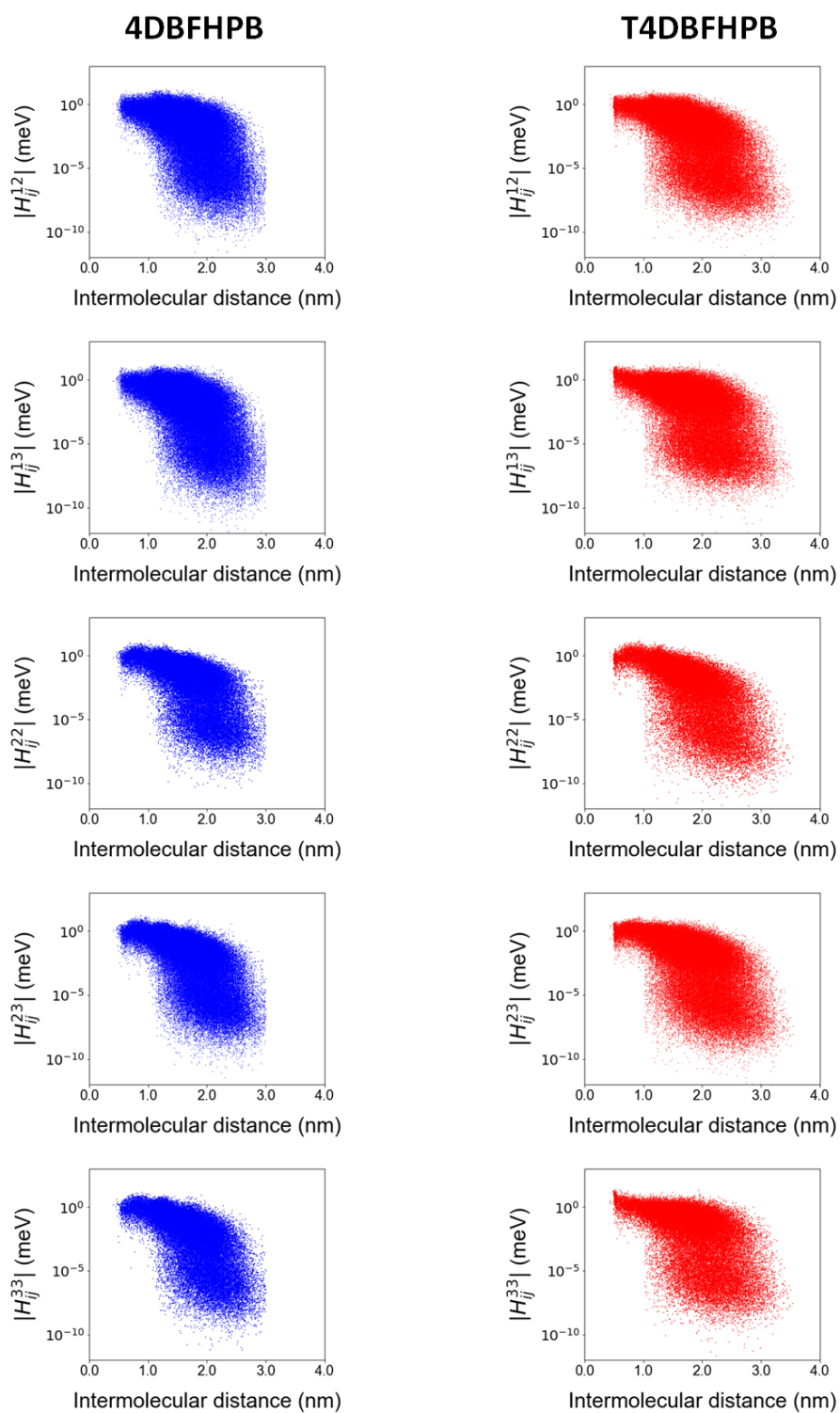


Figure S11. H_{ij}^{pq} vs. intermolecular distance. (continuation)

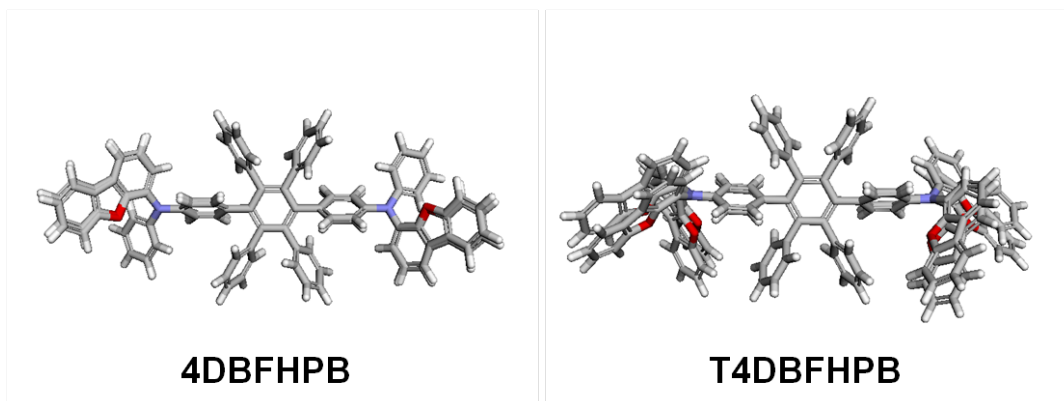


Figure S12. Differences between optimized geometries of neutral and cation states. Root-mean-square deviations (RMSD) of atomic positions were 0.150 Å and 1.16 Å in **4DBFHPB** and **T4DBFHPB** respectively.

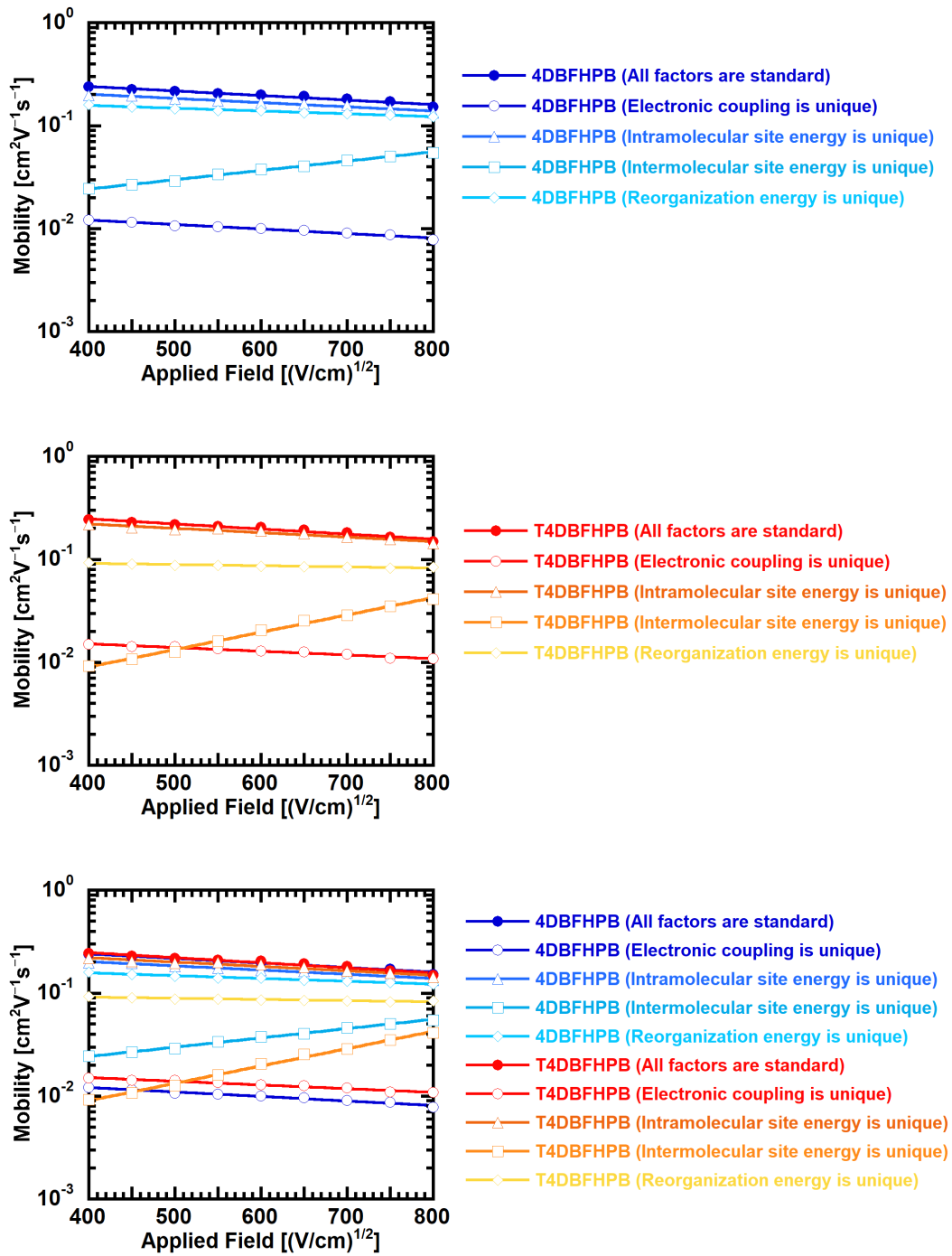


Figure S13. Simulated hole-mobilities. (The mobilities in the all-factors-are-standard and one-factor-is-unique conditions. $\lambda_{\text{standard}} = 100 \text{ meV}$.)

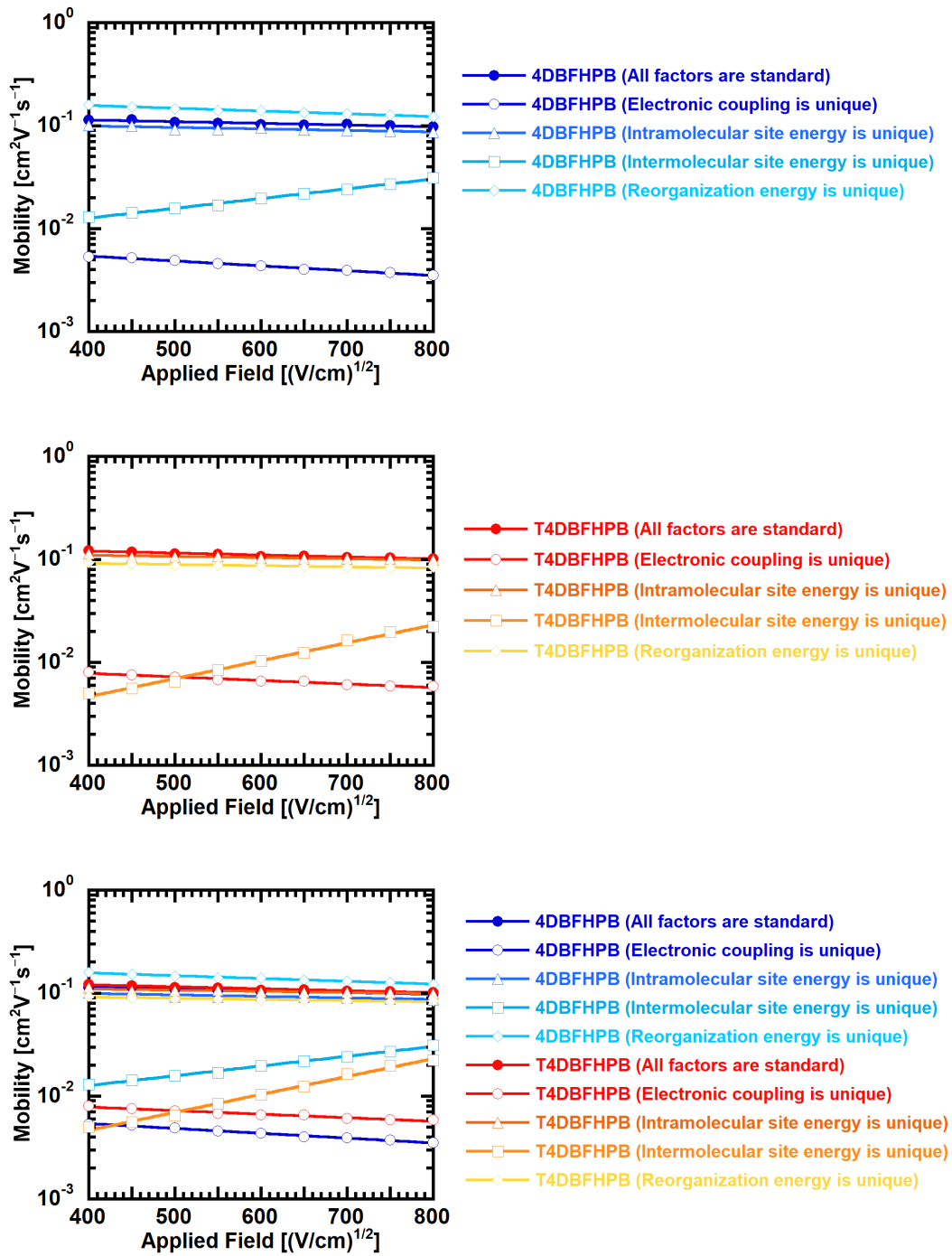
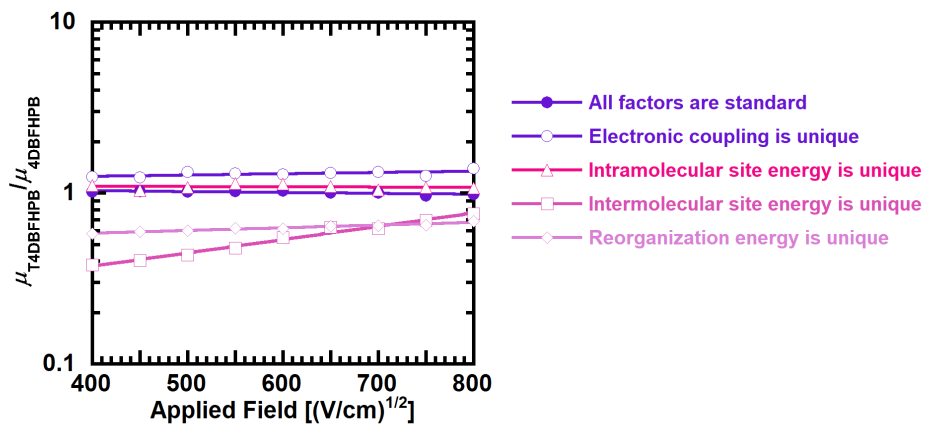


Figure S14. Simulated hole-mobilities. (The mobilities in the all-factors-are-standard and one-factor-is-unique conditions. $\lambda_{\text{standard}} = 155 \text{ meV}$.)

a)



b)

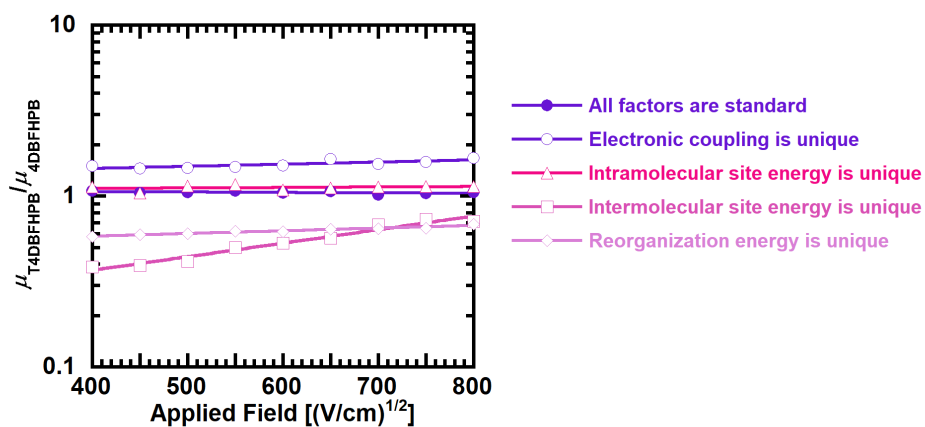


Figure S15. The difference between the simulated hole-mobilities of **T4DBFHPB** and **4DBFHPB**. (The ratios in the all-factors-are-standard and one-factor-is-unique conditions. a) $\lambda_{\text{standard}} = 100 \text{ meV}$, b) $\lambda_{\text{standard}} = 155 \text{ meV}$.)

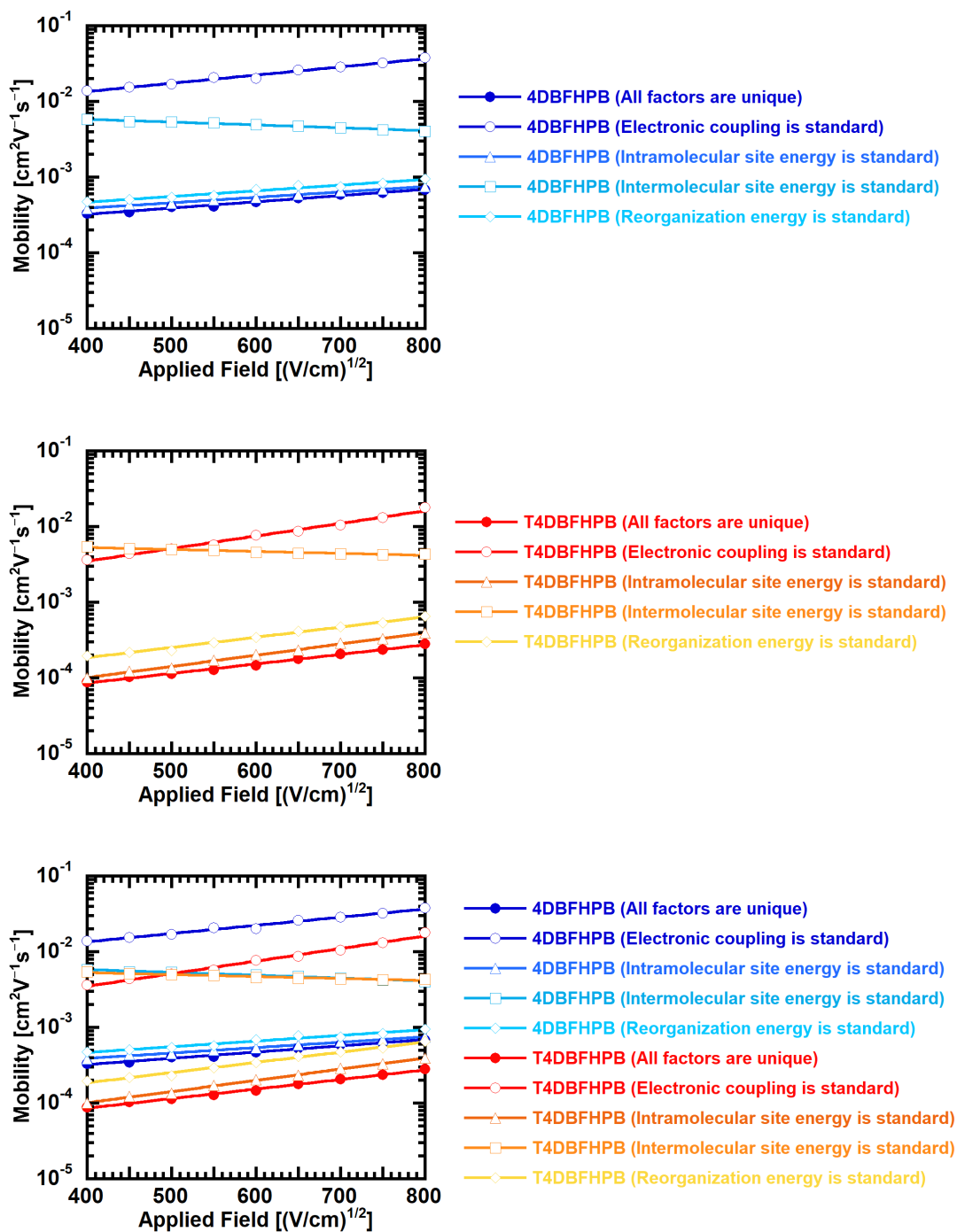


Figure S16. Simulated hole-mobilities. (The mobilities in the all-factors-are-unique and one-factor-is-standard conditions. $\lambda_{\text{standard}} = 100 \text{ meV}$.)

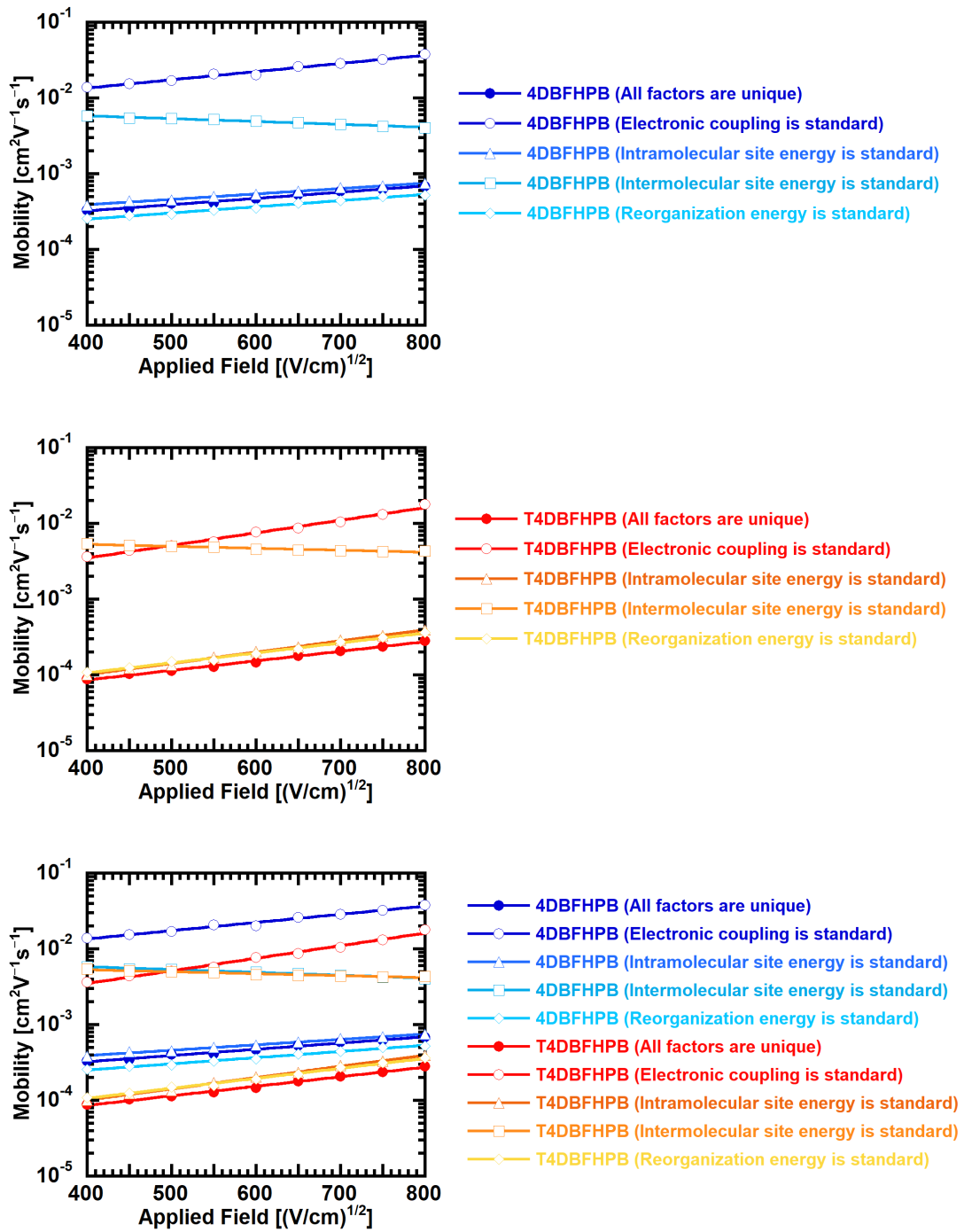


Figure S17. Simulated hole-mobilities. (The mobilities in the all-factors-are-unique and one-factor-is-standard conditions. $\lambda_{\text{standard}} = 155 \text{ meV}$.)

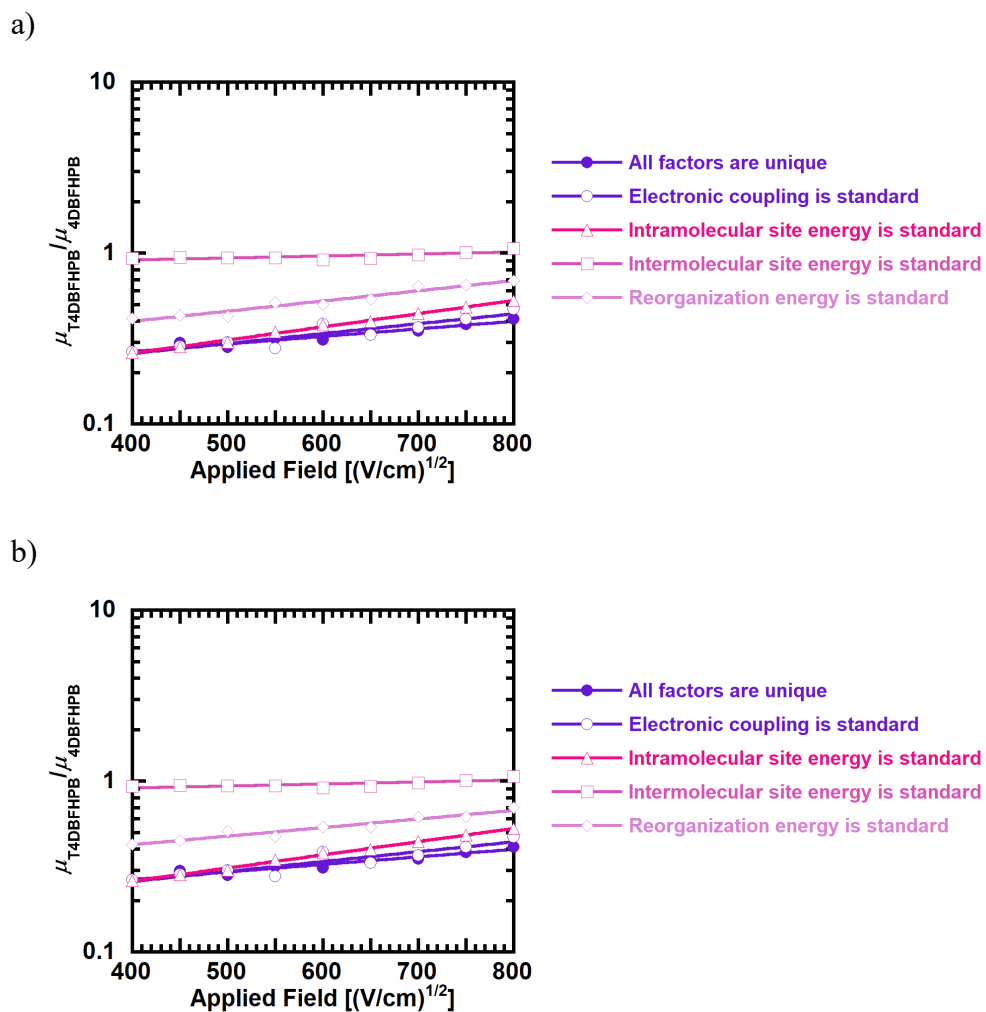


Figure S18. The difference between the simulated hole-mobilities of **T4DBFHPB** and **4DBFHPB**. (The ratios in the all-factors-are-unique and one-factor-is-standard conditions. a) $\lambda_{\text{standard}} = 100 \text{ meV}$, b) $\lambda_{\text{standard}} = 155 \text{ meV}$.)

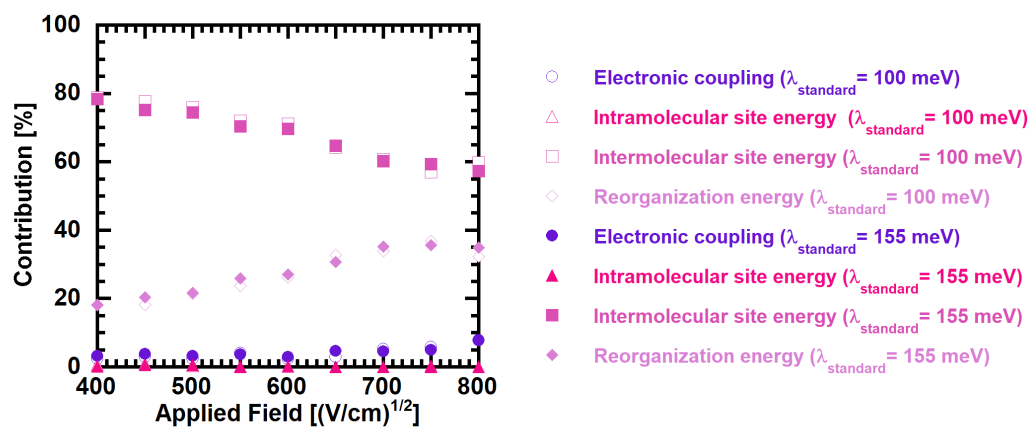
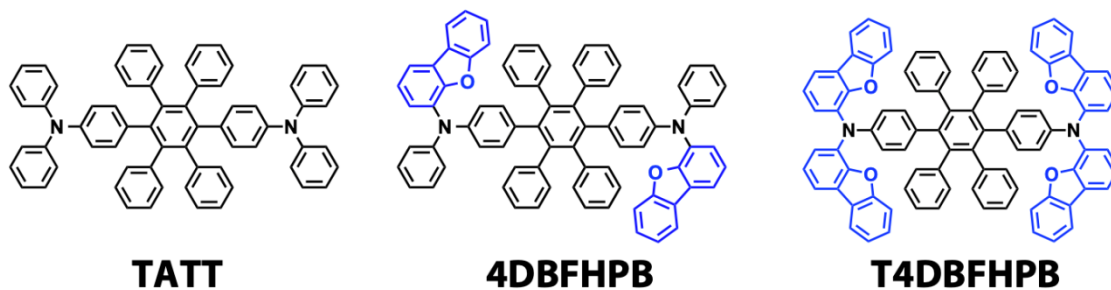


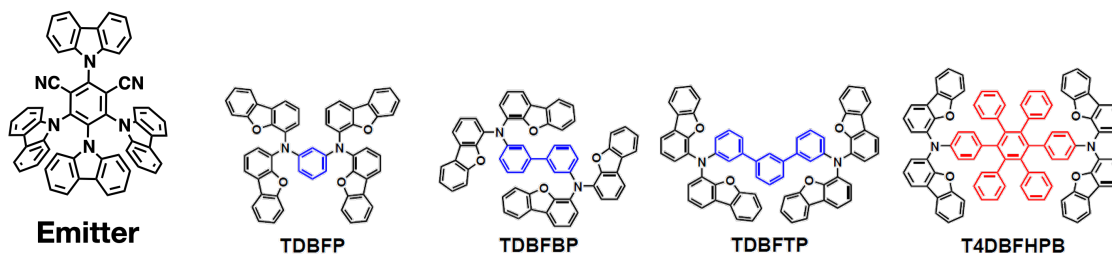
Figure S19. Governing factors for the difference between hole-mobilities of **4DBFHPB** and **T4DBFHPB**.

Table S3. OLED performances improved by the introduction of dibenzofuran end-capping groups.



HTM	V_{1000} (V)	$\eta_{\text{ext},1000}$ (%)	$\eta_{\text{p},1000}$ (lm W^{-1})	LT_{50} at 1000 cd m^{-2} (h)	LT_{95} at 1000 cd m^{-2} (h)
TATT	4.30	20.8	52.0	12,000	160
4DBFHPB	4.07	19.2	51.5	24,000	670
T4DBFHPB	3.83	22.0	62.2	28,000	430

Table S4. Efficacy of using HPB-core HTM as HTL of the TADF OLED.



EQE_{1000}	19.4%	23.0%	22.7%	22.0%
LT_{50} @1000 cd m^{-2}	~ 20,645 h	~ 17,366 h	~ 22,413 h	~ 28,000 h
V_{on}	2.35 V	2.40 V	2.42 V	2.41 V
V_{1000}	4.00 V	4.02 V	4.06 V	3.83 V

Table S5. Comparison of the thermal and optical properties.

HTM	Molecular weight	T_g (°C)	I_p (eV)	E_T (eV)	BDE (eV)
TDBFP	773	131	-5.6	2.7	1.56
TDBFBP	849	138	-5.7	2.7	1.61
TDBFTP	924	145	-5.7	2.7	1.60
T4DBFHPB	1229	171	-5.6	2.8	1.72

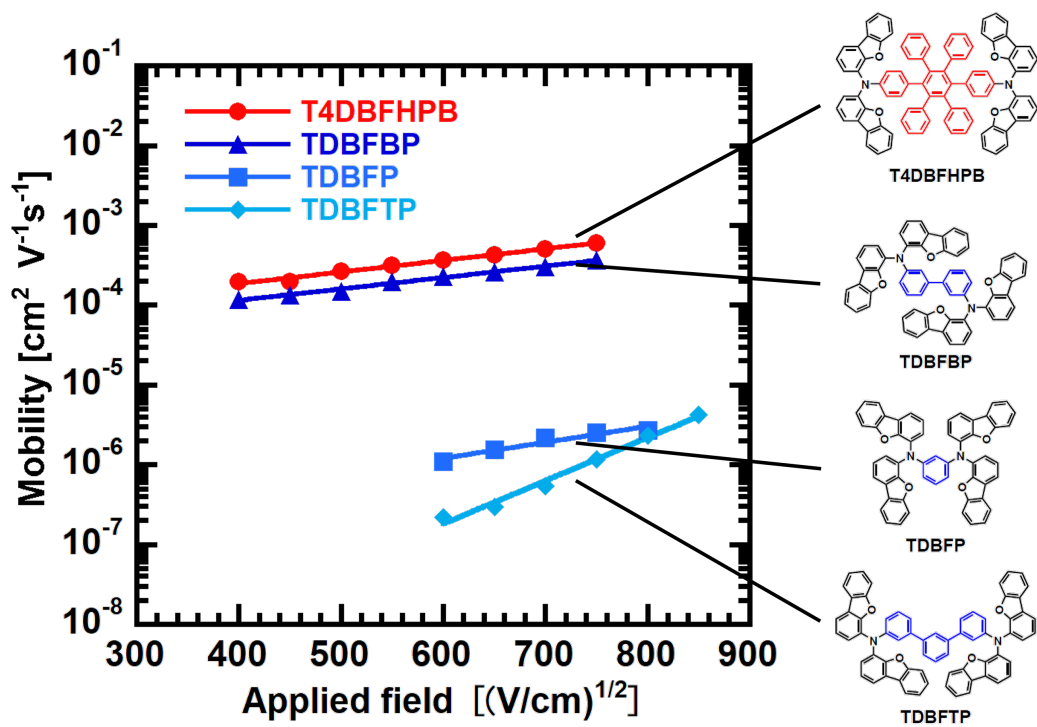


Figure S20. Superior mobility of the HPB-core HTM.

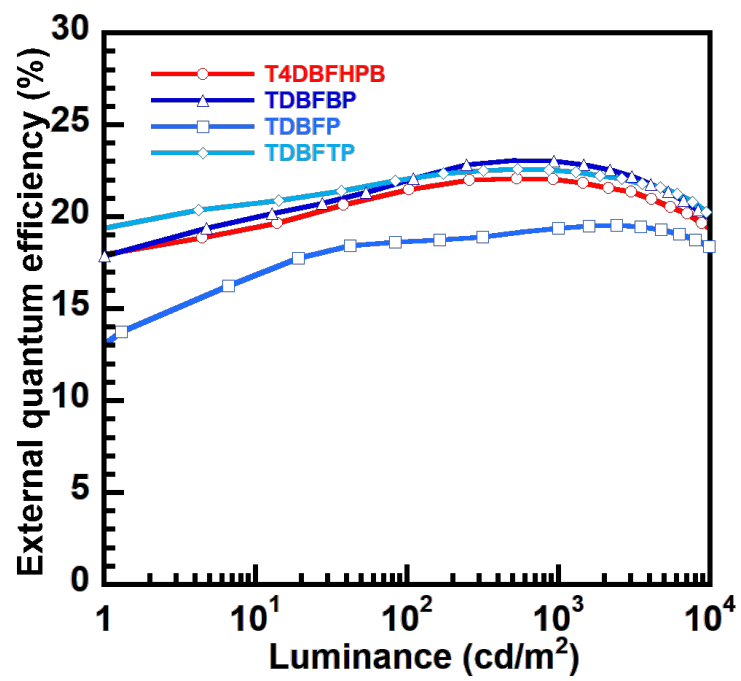


Figure S21. Comparison of the EQE.